Clays and Clay Minerals, Vol. 37, No. 2, 113–127, 1989.

APATITE REPLACEMENT AND RARE EARTH MOBILIZATION, FRACTIONATION, AND FIXATION DURING WEATHERING

JILLIAN F. BANFIELD[1] AND RICHARD A. EGGLETON

Geology Department, Australian National University
P.O. Box 4, Canberra City, 2601 A.C.T., Australia

Abstract—During an electron microscope study of the weathering of granite from southern New South Wales, Australia, an assemblage of minerals including florencite and rhabdophane was discovered replacing apatite. Light rare earth elements released from allanite early in weathering apparently combined with P released by leaching of primary apatite to form secondary phases exhibiting a range of morphologies and compositions. Chondrite normalized fractionation patterns La > Nd > Sm > Ce; La > Ce > Nd ≥ Sm and La = Sm = Nd > Ce were identified. The rare earth elements were present in very small crystals and aggregates of secondary minerals (<10 μm) and coexisted with clays and secondary Fe-Ti oxides. The weathered granite was enriched about 6 to 10 times in all rare earth elements except Ce relative to fresh granite if the abundances were corrected for apparent enrichment due to reduction in density. The rare earth elements were probably derived from higher in the weathering profile, possibly by destruction of florencite and rhabdophane in very intensively weathered rock. Ce remained relatively immobile during weathering, probably due to its oxidation to Ce^{4+}.

Key Words—Apatite, Florencite, Granite, Phosphorus, Rare earth elements, Rhabdophane, Scanning electron microscopy, Weathering.

INTRODUCTION

Some authors (e.g., Nance and Taylor, 1977; Hanson, 1980) have suggested that the rare earth elements (REE) are not readily fractionated under surficial conditions. This view has been refuted by studies that have demonstrated these elements can indeed be transported and fractionated during weathering (see, e.g., Vlasov, 1966; Burkov and Podporina, 1967; Krasil'nikov, 1969; Nesbitt, 1979; Duddy, 1980; Harris, 1985). Explanations for the reported behavior of the REE vary. Nesbitt (1979) suggested that fractionation of REE during weathering was due to adsorption of light rare earth elements (LREE) relative to heavy rare earth elements (HREE) on primary and secondary minerals. Duddy (1980) reported that REE are fixed by vermiculite, which has been found to contain as much as 10% La + Ce + Nd + Y. REE-phosphates have been identified in residual and phosphorite deposits, in weathering crusts, and in soils (e.g., Vlasov, 1966; Norrish, 1968).

Apatite weathering represents the major source of phosphorus for biological processes, sediments, and soils. The examination of the initial breakdown of igneous apatite is crucial to the understanding of the pathways of this element through the hydrosphere, biosphere, and lithosphere. Most studies of apatite weathering have focused on the alteration of carbonate-rich sedimentary phosphorite deposits, carbonatites, and guano (see review by Altschuler, 1973). Altschuler (1973) reported the reaction of carbonate-fluorapatite with clays to produce Ca(Na, K)-Al-phosphate and Al- or Fe-phosphate minerals, the compositions of which depended on the chemistry of the parent rock and degree of weathering. Flicoteaux and Lucas (1984) noted that acid conditions and the absence of carbonates in rocks promoted the breakdown of apatite, often leading to the formation of Fe- and Al-phosphates. They proposed that hydrous Fe-Al-phosphates formed either by adsorption of P onto clay minerals, or by a slow chemical etching of the clay structure accompanied by the precipitation of secondary minerals.

The weathering of apatite in igneous rocks having phosphorous contents equivalent to 1% apatite (~0.05% P_2O_5), however, has not been described in detail. This paper reports details of the morphology, mineralogy, and chemistry of the weathering products of primary apatite in such a rock, and illustrates the complex manner in which rare earth elements may be fractionated during weathering.

EXPERIMENTAL

Samples

Samples of fresh and progressively weathered granite were collected from a profile exposed near the base of a road-cut in the I-type (Chappell and White, 1974) Bemboka granodiorite, near Brown Mountain, on the Snowy Mountains Highway between Cooma and Bega, southern New South Wales, Australia [Figure 1 (left)]. The samples were collected outward from the central areas of increasingly weathered granite tors [Figures 1 (center) and 1 (right)]. The fresh rock contained plagioclase, K-feldspar, quartz, biotite, minor amphibole, and accessory zircon, apatite, allanite, and, possibly, thorite. The granite also contained small amounts of epidote,

[1] Present address: Department of Earth and Planetary Sciences, The Johns Hopkins University, Baltimore, Maryland 21218.

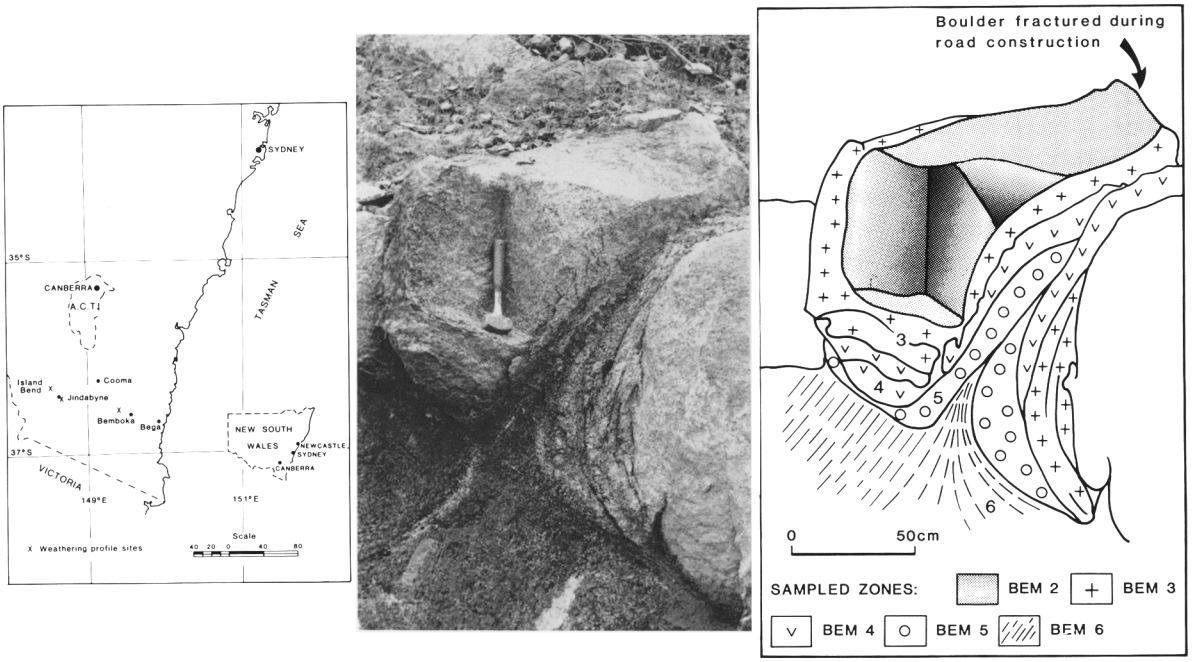

Figure 1. (left) Location of the Bemboka and Island Bend weathering profiles in southern New South Wales, Australia. (center) Photograph of weathered granite boulders after samples had been collected. (right) Diagram illustrating the regions from the area shown in Figure 1b where individual samples were collected.

chlorite, muscovite, and titanite, thought to be low-temperature hydrothermal alteration products.

Materials examined in this study ranged from fresh granite having a density of 2.7 g/cm^3, to highly weathered granite having a density of about 1.8 g/cm^3. Decreasing density of the samples appeared to correlate directly with the intensity of weathering. In moderately weathered samples, biotite was replaced largely by vermiculite, amphibole was partly replaced by smectite and iron oxide, and plagioclase was extensively altered to halloysite. In highly weathered samples, biotite and vermiculite were replaced by kaolinite and goethite, plagioclase was completely replaced by halloysite and kaolinite, and K-feldspar was deeply etched and converted to kaolinite. The highly weathered samples were extremely porous, but retained the original granitic texture. Thus, the weathering of the granite probably occurred without expansion or contraction of the granitic fabric, i.e., isovolumetrically.

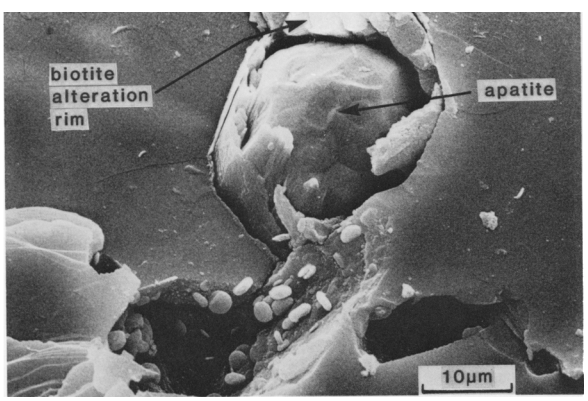

Figure 2. Scanning electron micrograph of an etched apatite crystal and replacement rind.

Biotite in the fresh granite contained euhedral apatite crystals as long as 60 μm. Biotite was handpicked from the crushed granite and split along cleavage planes with a razor blade to expose basal planes from the interiors of crystals. To minimize contamination, the samples were immediately lightly coated with carbon or gold and examined in the scanning electron microscope (SEM). Partially weathered biotite contained hexagonal and prismatic pits formed by the dissolution of these apatite crystals. It is in these pits that secondary phases were observed in the SEM. At least 100 examples of coexisting apatite and secondary minerals from six samples displaying different degrees of weathering were examined in this study. Apatite crystals from a second profile in the Island Bend granite (Figure 1a) were also examined to test whether the observations from the Bemboka profile were the result of a unique process or represent a more general phenomenon.

Electron microscopy

Biotite crystals containing partly and completely weathered apatite crystals were examined in a Cambridge Stereoscan 180 scanning electron microscope operated at 30 kV. An energy dispersive X-ray spectroscopic system (EDX) allowed qualitative chemical analysis of the apatite and its alteration products. Material firmly attached to pit walls was removed under a light microscope using a fine needle and examined separately by X-ray powder diffraction (XRD) and transmission electron microscopy (TEM). Electron images and diffraction patterns were obtained using JEOL 100CX and 200B transmission electron microscopes. A scanning-transmission electron microscope (STEM) fitted with EDX was used to confirm the identity and to examine the composition of some of the TEM samples. The SEM was used to locate material which was then extracted and examined by optical microscopy.

https://doi.org/10.1346/CCMN.1989.0370202 Published online by Cambridge University Press

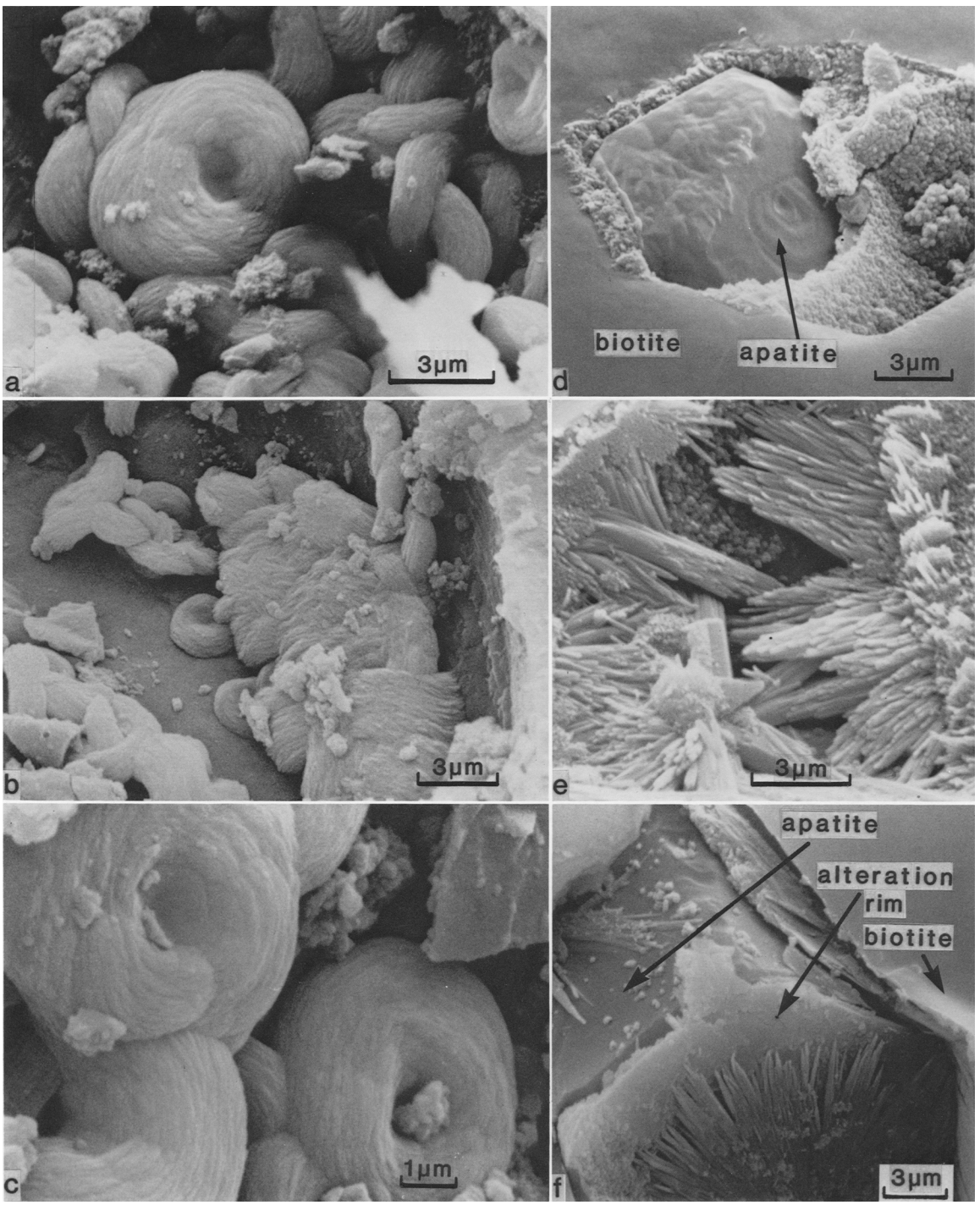

Figure 3. Scanning electron micrographs showing alteration products formed by replacement of apatite: (a) donut-shaped aggregates; (b) intermeshed donut-shaped alteration products; (c) irregular surfaces on donut-shaped particles; (d) knobbly rind on an etched apatite crystal enclosed in biotite; (e) aggregate of elongate crystals; (f) elongate crystals on the altered surface of an apatite crystal enclosed in biotite.

X-ray powder diffraction

A very small amount ($\ll 1$ μg) of apatite alteration products was collected onto the end of a fine glass spindle, and X-rayed with CoKα radiation in a 114-mm Gandolfi camera.

Elemental analyses

Elemental abundances in mineral and clay separates and in whole rock samples were determined by neutron activation analysis (NAA). Samples (~350 mg) were irradiated in a ther-

https://doi.org/10.1346/CCMN.1989.0370202 Published online by Cambridge University Press

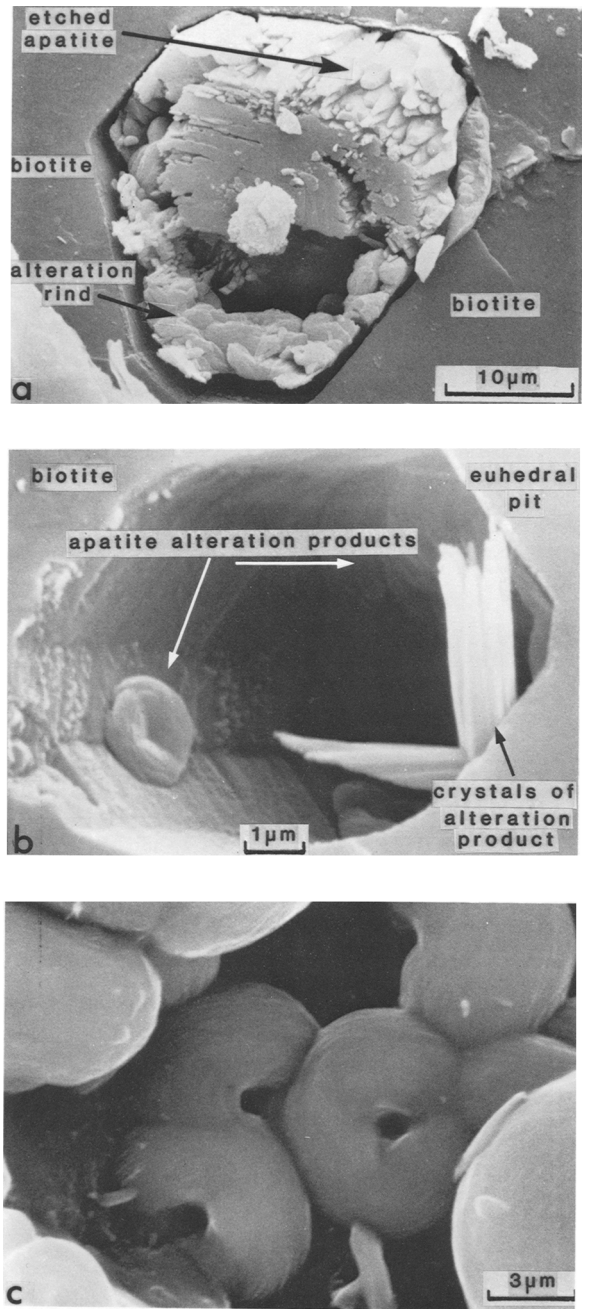

Figure 4. Scanning electron micrographs of: (a) etched apatite crystal in biotite, with donut-shaped particles in an alteration rind; (b) co-existing donut-shaped particles and crystals in a pit in biotite; (c) aggregate of donut-shaped particles with central holes.

mal neutron flux of 4 × 10^{12} n/cm²/s for 24 hr; six counts were taken at intervals over a period of six months. REE analyses were obtained for 14 samples, including six whole rock samples from the Bemboka profile that showed varying degrees of weathering, three clay samples extracted from the most weathered members of this sequence, and fresh and moderately weathered biotite separates. Three samples from the Island Bend granite weathering profile were also analyzed in this manner.

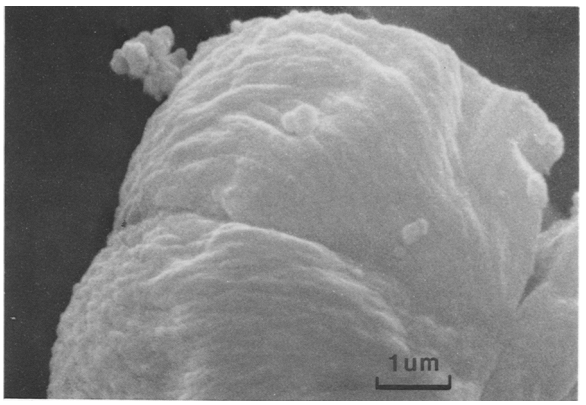

Figure 5. Scanning electron micrograph of the fractured surface of a large aggregate of alteration product.

The chemical compositions of the minerals replacing apatite were determined using a wavelength-dispersive CAMECA electron microprobe. As data were collected from irregular surfaces and from deep within pits, the results are only semi-quantitative.

RESULTS

Morphology of alteration products

Early-stage weathering of apatite crystals resulted in the development of etch pits and replacement rinds (Figure 2). As weathering proceeded the apatite was found to be increasingly replaced by a variety of secondary phases, which can be seen as rims, donut-shaped aggregates, and euhedral crystals (Figures 3a–3f). Donut-shape aggregates were locally present within what appears to be an alteration rind (Figure 4a). Donut-shape particles and crystals of secondary minerals were rarely found in the same pit; Figure 4b shows one of the only pits in which they coexist.

Figures 3a–3c illustrate that the surfaces of donuts were covered with concentric ridges. Donuts commonly had a central circular depression, some had a complete central hole (Figure 4c), and many resembled a flattened helix. In Figure 5, the internal structure dominated by radiating crystals suggests that the morphology of alteration products was controlled by their internal organization.

Donut and rim mineralogy of florencite

X-ray powder diffraction. The d-values of an aggregate of alteration products obtained by XRD are listed in Table 1. Most d-values could be assigned to florencite, a hydrous, light-rare-earth-element Al-phosphate, and apatite. The remaining strong reflections at 4.2 and 3.7 Å could not be attributed to either of these phases or uniquely to any other mineral.

Chemistry. Qualitative EDX data indicate that donuts and rims consist chiefly of La, Ce, Nd, Sm, Al, and P

https://doi.org/10.1346/CCMN.1989.0370202 Published online by Cambridge University Press

Table 1. X-ray powder diffraction data for apatite (a) alteration products, including florencite (f) and an unidentified mineral (?).

d-values (Å)	Intensity (I/Io)[1]	Mineral
5.65	9	f
4.18	10	?
3.72	6	?
3.50	4	f
3.40	4	a
3.18	3	a
3.07	3	a
2.93	5	a, f
2.81	9	a, f
2.77	5	a
2.71	5	a, f
2.63	4	a
2.60	1	?
2.39	3	f
2.25	3	a, f
2.14	1	a, f
2.03	1	a, f
1.94	3	a
1.88	5	a, f
1.84	5	a
1.80	3	a
1.77	1	a
1.75	1	a, f
1.72	1	a
1.68	1	a, f

[1] Relative intensities were difficult to estimate as data were obtained from a minute quantity of material collected onto a glass spindle (a few cubic micrometers of sample).

and smaller amounts of Fe, Ca, Ba, Pb, and HREE. Chemical data from alteration products (Table 2) are consistent with the XRD identification of florencite, written:

$$(La, Ce, Nd, Sm, Ba, Ca, Fe, Pb)Al_3(PO_4)_2(OH)_6.$$

Optical microscopy. In plane polarized light the donut-shaped particles were transparent pale-yellowish-green, non-pleochroic, and had refractive indices of 1.52–1.6. Under crossed polars these particles had first-order gray birefringence, and on rotation they produced an extinction pattern similar to a biaxial positive interference figure, with a simulated 2V of about 30°. This apparent interference figure is not completely understood.

Transmission electron microscopy. Images and diffraction patterns from thin slivers of alteration products revealed that the donuts were composed of aggregates of radiating crystals surrounded by very fine particles of crystalline material. Figures 6a and 6b further illustrate the presence of domains of a phase having a very fine net or cell-like appearance. Electron diffraction patterns of this material contain a few broad rings (Figure 6c), which exhibit strong preferred orientation, consistent with the presence of many small units arranged in a regular manner. Single crystal spots were also present in many diffraction patterns, typically superimposed on the powder rings, and displaying a regular relationship to the maxima and minima in them (Figure 6d and 6f). Dark field images obtained using single crystal reflections show prismatic laths commonly longer than 1000 Å. A bright field image of these radiating laths is shown in Figure 6e. Some electron diffraction patterns of alteration products showed additional reflections at about 4.2 and 3.7 Å, which are incompatible with florencite (Figure 6d). These reflections were common perpendicular or parallel to maxima in the powder rings or spots, suggesting the presence of a second phase in an orientation that is crystallographically controlled by the first material.

Table 2. Microprobe analyses (wt. %) of florencite and apatite from Bemboka 4.

Sample	La_2O_3	Ce_2O_3	Nd_2O_3	Sm_2O_3	BaO	CaO	FeO	P_2O_5	Al_2O_3	Total
					Type-1 florencite: La ≫ Ce					
14	15.8	1.1	4.0	0.7	1.8	1.0	1.7	10.8	26.2	63
15	15.6	1.2	5.0	0.8	2.2	1.1	1.7	11.6	39.7	79
16	16.3	1.6	4.9	0.9	2.2	1.0	2.4	22.4	34.1	86
18	13.9	1.1	4.7	0.8	1.1	0.9	2.5	22.6	36.7	84
19	11.8	0.7	3.7	0.5	0.0	0.7	3.3	15.2	26.4	62
2	18.0	0.8	5.5	0.9	1.3	8.5	2.5	22.1	33.4	93
3	11.4	1.1	3.2	0.6	1.0	0.9	3.8	17.9	33.4	73
5	13.9	2.6	4.1	0.6	2.1	0.6	2.7	26.8	45.0	98
23	16.0	1.7	4.7	0.9	3.0	3.5	2.0	8.1	22.8	63
4	16.8	0.8	4.9	0.8	2.0	2.9	4.6	18.1	30.1	81
					Type-2 florencite: La ≈ Ce					
12	5.9	6.5	4.6	1.2	4.0	1.1	1.9	11.8	36.7	74
13	4.0	8.3	4.9	1.6	1.6	0.7	3.1	8.0	25.0	57
6	3.7	5.7	1.0	0.7	5.4	1.3	1.5	28.9	44.3	93
7	3.2	5.7	1.9	0.6	7.2	2.2	1.3	27.5	35.0	85
8	3.9	6.6	2.6	0.7	5.5	1.7	1.9	20.1	44.7	88
21	3.5	5.7	2.9	0.6	0.3	1.1	3.6	16.1	28.0	62
25	5.2	4.6	4.2	1.1	Ti	0.9	6.6	15.4	40.2	78
26	6.1	5.8	4.0	0.9	3.5	3.2	12.5	11.3	45.4	93
Apatite	0.1	0.3	0.2	0.1	0.0	56.2	0.6	42.5	0.0	100

https://doi.org/10.1346/CCMN.1989.0370202 Published online by Cambridge University Press

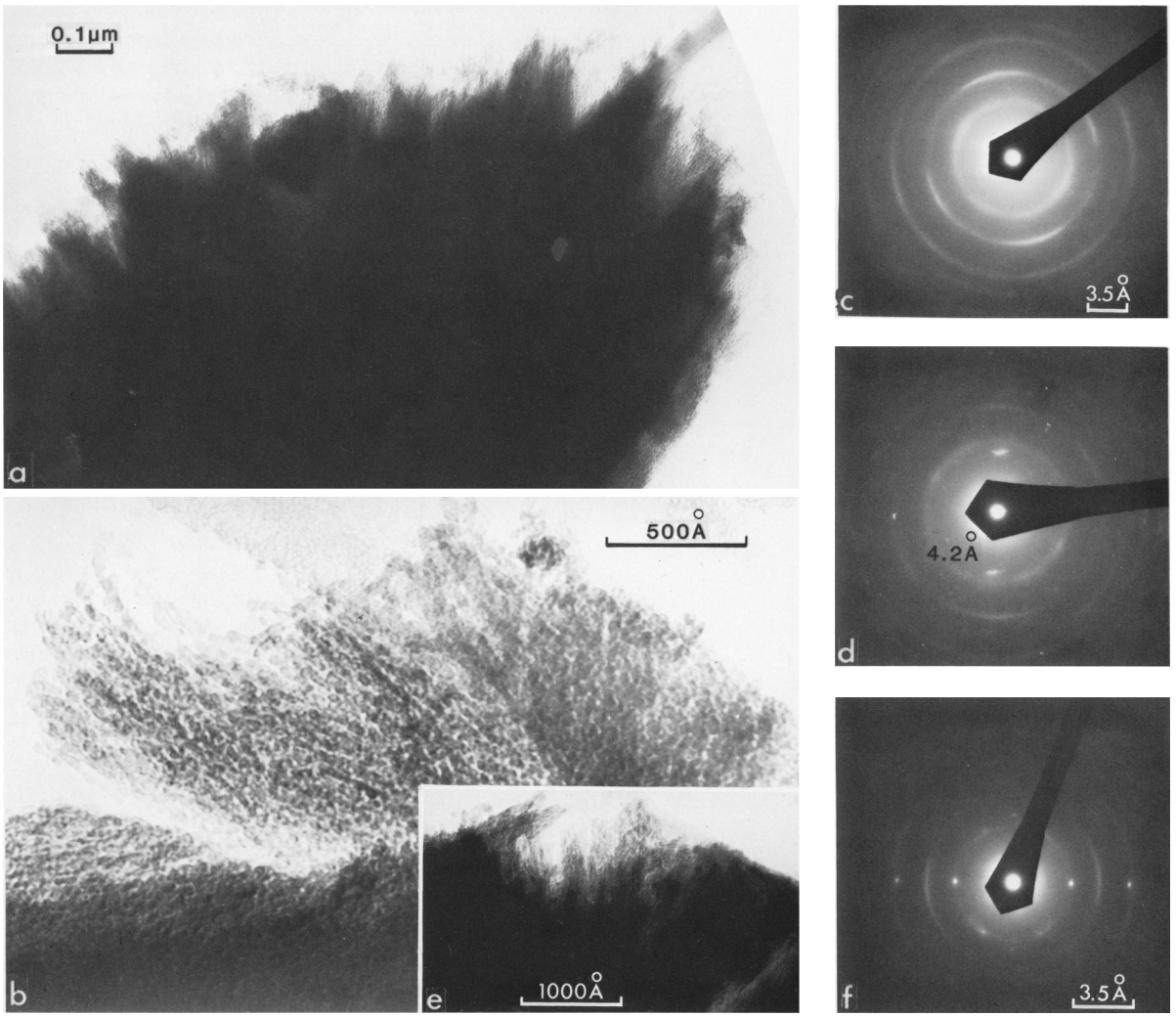

Figure 6. Transmission electron micrographs and electron diffraction patterns of alteration products: (a) cluster of radiating fibers mounted on a holey carbon grid; (b) higher magnification image of material in (a) revealing a cell-like texture; (c) electron diffraction pattern containing broad rings having intensity distributions suggestive of aggregates of minute crystals with preferred orientations; (d) electron diffraction pattern containing single crystal reflections at 4.2 and 3.75 Å; (e) bright-field image of larger crystals about 1000 Å in length; (f) electron diffraction pattern containing single crystal reflections, commonly superimposed on powder rings.

Euhedral crystals replacing apatite: rhabdophane

Crystals illustrated in Figure 7 were extracted and identified as rhabdophane using electron diffraction data. The Z*-[110] and X*-Z* zones are shown in Figures 8a–8c. Rhabdophane, commonly written as $CePO_4 \cdot H_2O$, is a hexagonal, low-temperature analogue of monoclinic monazite (Mooney, 1950). The hexagonal nature of the crystals shown in Figure 8d is apparent. An EDX spectrum from crystals in Figure 8a is shown in Figure 8e. The spectrum contains large Nd and La peaks and virtually no Ce peak. Bowles and Morgan (1984) reported similar Nd-dominated compositions and noted that rhabdophane from magmatic rocks tends to be more Ce rich than that from sediments and limonitic ores, which contain significant Nd.

Unidentified crystals replacing apatite

A second type of prismatic crystals was noted on a REE-Al-phosphate rind (Figure 9). Electron microprobe analyses indicated that these crystals contained no significant P, but were rich in Al and REE, particularly La, Nd, and Sm (see Figure 10). The oxide totals for this material were low (50–72%), suggesting that this phase may contain CO_2, F, H_2O, or some combination of these.

https://doi.org/10.1346/CCMN.1989.0370202 Published online by Cambridge University Press

Table 3. Analyses from Table 2 expressed as percentage of florencite and percentage of excess oxides.

Sample	(1) Florencite (%)	(2) REE + Ca + Ba excess (%)	(3) Al + Fe excess (%)	(4) REE atomic ratios La:Ce:Nd:Sm			
Type-1 florencite							
15	50	18	33	69	5	22	4
14	60	21	23	73	5	19	3
4	74	14	15	72	4	21	4
19	76	3	17[1]	71	4	22	3
3	74	1	21	70	7	20	4
2	78	15	11	71	3	22	4
18	82	0	27	68	6	23	4
5	82	0	17	66	12	19	3
16	83	5	12	69	7	21	4
Type 2-florencite							
26	40	18	36[1]	36	35	24	6
12	50	20	33	33	36	25	7
13	50	26	29	21	44	26	8
25	60	0	31[1]	34	31	28	7
8	69	0	26	28	50	19	5
21	78	0	19	27	45	23	5
6	90	0	13	33	51	9	6
7	96	6	6	28	50	17	5

[1] Coexist with Fe-Ti oxides.

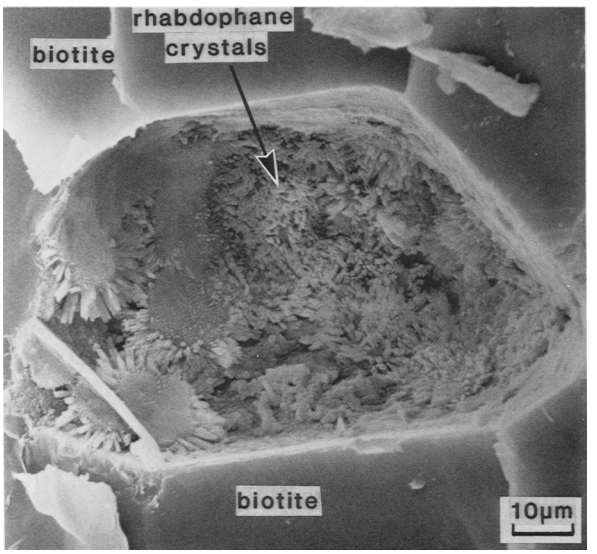

Figure 7. Scanning electron microscope micrograph of very small crystals within a pit in biotite. These crystals were extracted and identified by electron diffraction and analytical electron microscopy as rhabdophane (see Figure 8).

Chemistry of donut and rim alteration products

Semiquantitative electron microprobe data for apatite and florencite are listed in Table 2. Probe totals generally range between 80% and 100%. A mean value for the alteration products of about 89% is close to that expected for florencite. The data in Table 2 are divided into two groups on the basis of the relative abundances of LREE. Although the two varieties of florencite were also distinguishable on the basis of their total REE and Ba contents, they could not be distinguished morphologically. Within a single biotite crystal, pits containing both types of florencite were identified. Type-1 florencite contained very abundant La_2O_3, and very little Ce_2O_3, whereas Ce_2O_3 constitutes as much as half the LREE assemblage in type-2 florencite. Type-2 florencite was enriched in Ba and Ca and was characterized by a lower total REE content than type-1 florencite. The relative abundances of LREE in the two types of florencite differed significantly from the LREE distribution pattern obtained from the prismatic crystals (which were developed on a substrate of the more Ce-rich, type-2 florencite). These three LREE fractionation patterns, plotted in Figure 10, have been normalized to chondritic REE abundances.

Overall, the chemical data displayed large variations in the relative abundances of REE, Al, P, Ba, Fe, and Ca. Assuming that florencite was the major component of alteration products, the data in Table 2 were converted to molecular proportions using a formula based on 22 oxygens. For almost all samples, insufficient phosphorus was present for the analyses to represent only florencite. The remaining quantities of Al and REE are listed in Table 3 with the proportion of each analysis that could be expressed as florencite and the associated La:Ce:Nd:Sm ratio of the sample.

Neutron activation results

NAA of samples from the Bemboka and Island Bend profiles are shown in Table 4. The results for increasingly weathered granite have been converted from weight-based data to abundances expressed in g/cm^3, using measured sample densities. By assuming that weathering was isovolumetrical (Gardner *et al.*, 1978, 1981), direct comparison of volume-based abundances in fresh and weathered samples can be made to indicate whether an element had been added or lost from a profile. By normalizing the results to the fresh rock, changes resulting from weathering were revealed. In Figure 11 the results for each sample are plotted against the sample density.

To determine whether enrichment of the profile was related to a fractionation of the REE (other than Ce, which is clearly strongly fractionated from the other REE), data normalized to fresh rock were plotted for all REE determined (Figure 12). This method of presentation is analogous to chondrite normalization; results reflect the change in relative abundances of REE as a result of the process studied. The net effect of apatite replacement can also be determined by comparing the REE contents of weathered and unweathered biotite. This comparison is illustrated in Figure 12, where the REE content of unweathered biotite has been

https://doi.org/10.1346/CCMN.1989.0370202 Published online by Cambridge University Press

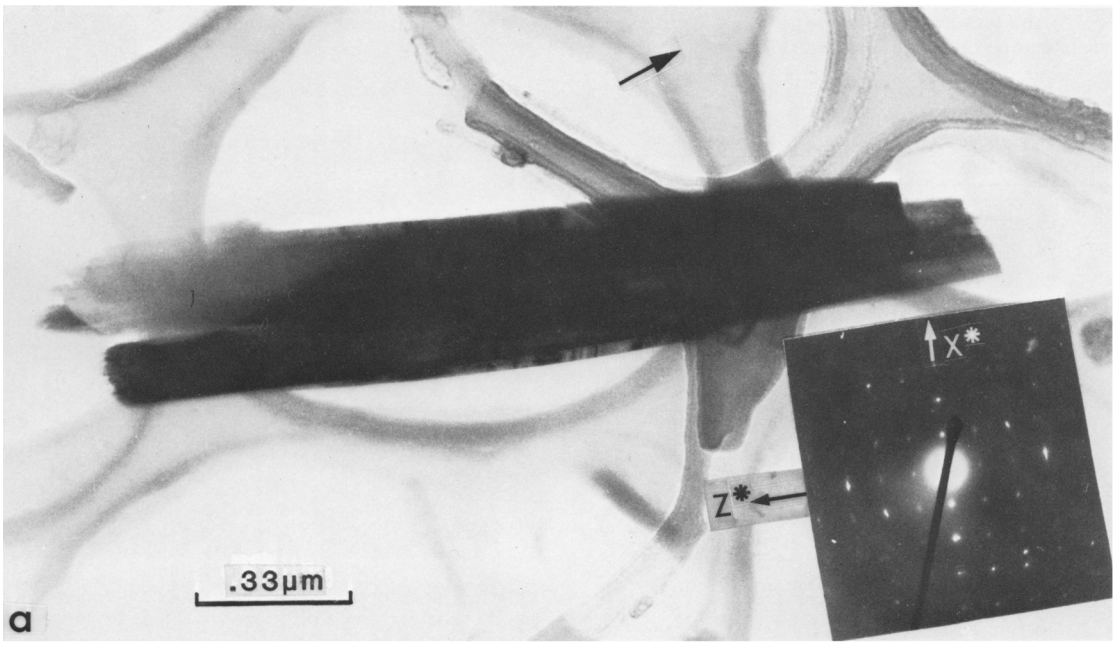

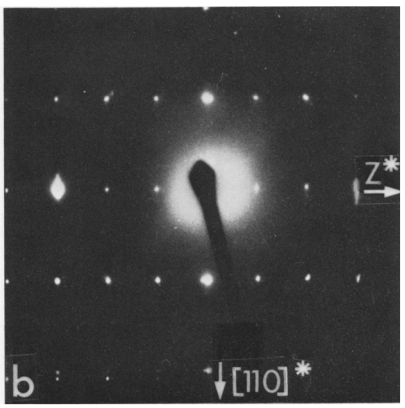

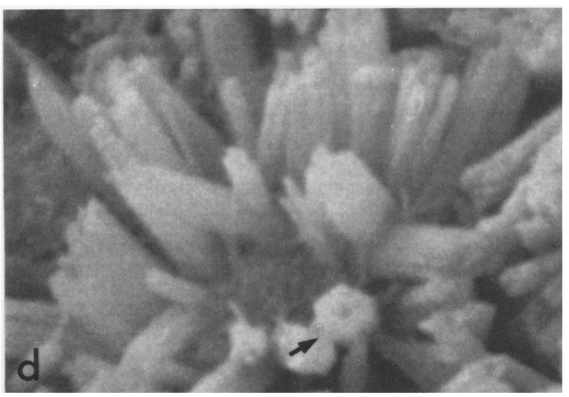

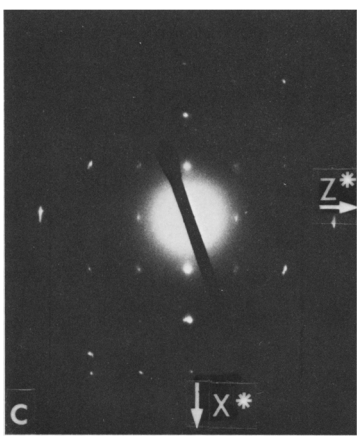

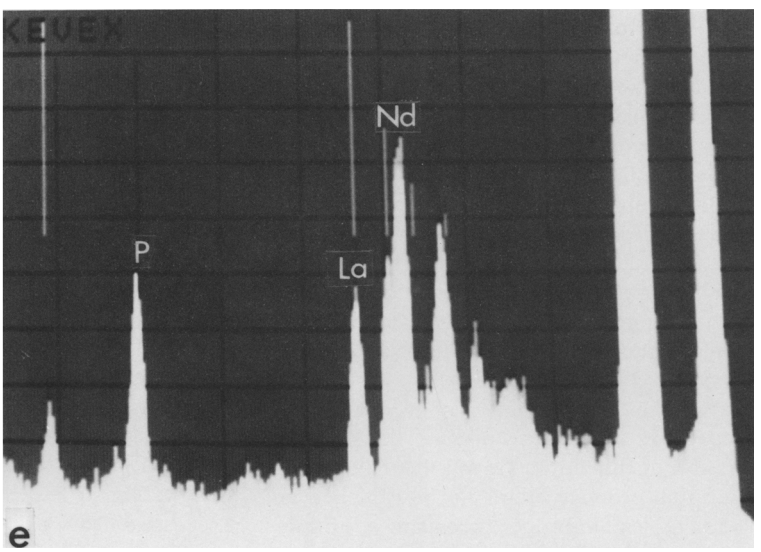

https://doi.org/10.1346/CCMN.1989.0370202 Published online by Cambridge University Press

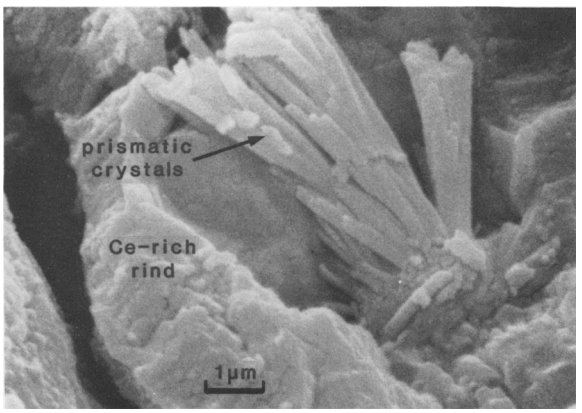

Figure 9. Scanning electron micrograph of crystals having a light rare earth element-Al composition, on a type-2 florencite replacement rind (see text).

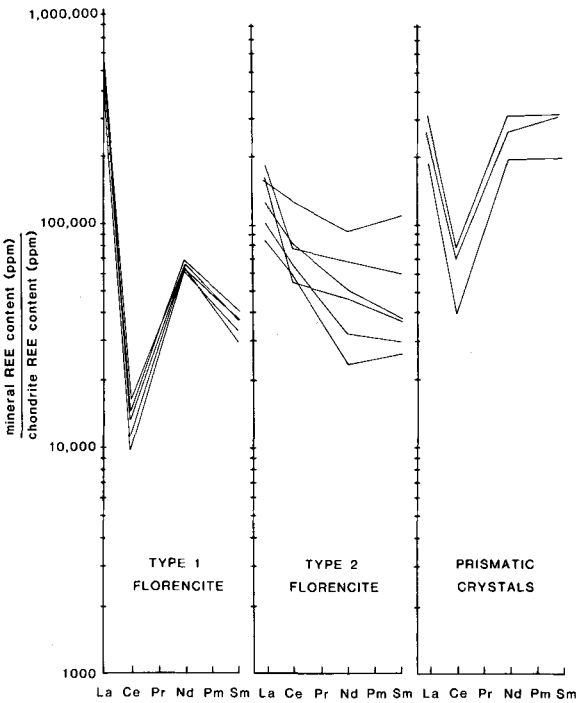

Figure 10. Chondrite-normalized rare earth element fractionation patterns for replacement phases, illustrating differences in relative contents of light rare earth elements.

subtracted from that of the weathered biotite and the result normalized to fresh rock REE contents.

The distribution of REE between the clay and non-clay fraction in a moderately weathered sample (Bemboka 4) is illustrated in Figure 13. Table 5 indicates the distribution of REE between minerals in different fractions of this sample. In column 1 of Table 5 the percentage of the total abundance of each REE that can be accounted for by replacement of apatite within the 10% modal biotite in the granite has been calculated using the biotite composition determined by NAA (Table 4). Column 2 lists the percentage of the REE content accommodated by the clay fraction. This proportion was determined using the analysis of Bemboka 4 clay (see Table 4) and the percentage clay in the sample (determined to be 9% by particle size analysis). Column 3 in Table 5 lists the percentage of REE in the whole rock that can not be accounted for by replacement of apatite in biotite or by the clay fraction (Total REE − columns 1 and 2).

The NAA results for fresh and weathered granite and the clay fraction from weathered material in the Island Bend profile plotted in Figure 14 show that a slight fractionation of the REE has occurred. MREE and HREE have been slightly enriched in the profile, and La was conserved. The plot contains a negative Ce anomaly. Results for the clay fraction indicate that as in the Bemboka profile, Ce was strongly associated with clay-sized materials. The heavier REE also show some tendency to concentrate separately from the lighter REE, possibly partitioning more strongly into the clay fraction. The behavior of the REE in the Island Bend profile was similar to that observed in the Bemboka profile, the major difference being the far less extreme nature of the enrichment process.

DISCUSSION

Mineralogy of alteration products

The SEM observations suggest that the alteration of apatite by dissolution and exchange of chemical components (e.g., Ca and REE) with fluid commenced in the early stages of weathering and resulted in a complex assemblage of secondary minerals, which exhibit a variety of morphologies and compositions. In addition to the crystallization of rhabdophane and two chemically distinct types of florencite, microprobe analyses (Tables 2, 3), electron diffraction patterns (Figure 6f), and XRD data (Table 1) suggest that another weathering product coexists with florencite. The results in Table 3 indicate that the % REE and % Al in excess of that required for florencite are broadly similar, suggesting that if a second phase is present, it may contain REE and Al in the proportions of roughly 1:3. La:Ce:

←

Figure 8. (a) Transmission electron micrograph of a rhabdophane crystal mounted on a holey carbon grid; (b, c) electron diffraction patterns of *hkl* and *h0l* nets from rhabdophane; (d) scanning electron micrograph of crystals before extraction from pit, exhibiting hexagonal crystal form; (e) scanning-transmission electron microscope energy-dispersive X-ray scan indicating a La-Nd-P composition.

https://doi.org/10.1346/CCMN.1989.0370202 Published online by Cambridge University Press

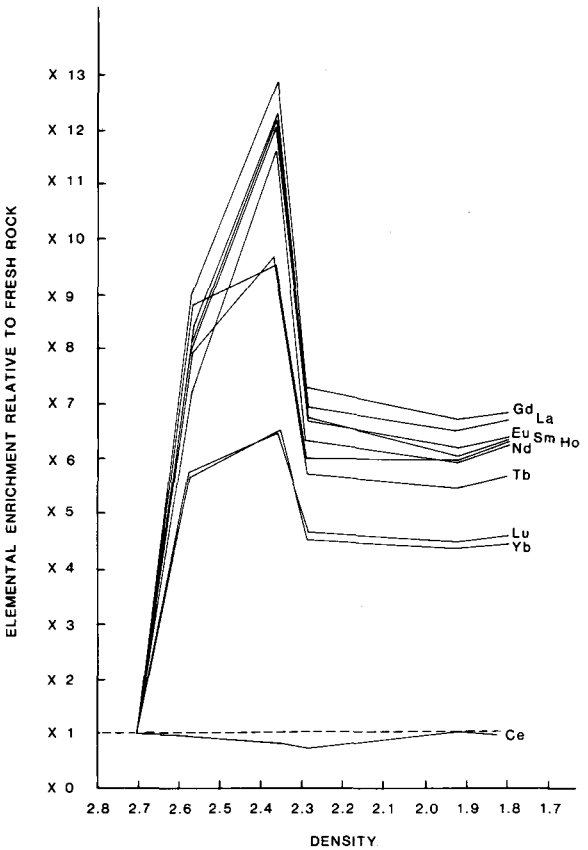

Figure 11. Rare earth element enrichment in samples from the Bemboka profile vs. rock density. Volumetric abundances have been normalized using volume-based abundances in fresh rock. Dashed line represents plot for an element that was neither added to, or lost from the profile during weathering.

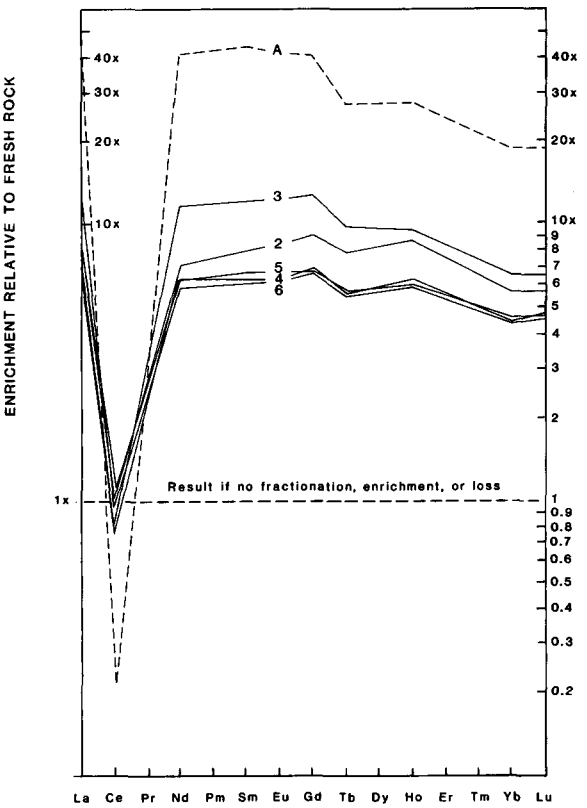

Figure 12. Enrichment of individual rare earth elements in slightly (2), moderately (3, 4), and strongly (5, 6) weathered Bemboka granite. Line A is the enrichment in biotite from (4), relative to fresh rock. For A to represent the actual contribution of apatite replacement to the overall enrichment, plot must be scaled down by factors representing the biotite content of the rock and amount of apatite in the rock that is not present as inclusion in biotite.

Nd:Sm ratios listed in Table 3 do not show a clear or consistent variation if excess REE and Al are present. If another REE-bearing phase is present, its REE distribution pattern does not differ markedly from that of the coexisting florencite.

The existence of at least four different REE-bearing alteration products in close spatial proximity has been established. The variety of alteration products may reflect different chemical environments under which crystallization proceeded. Alternatively, the different secondary minerals may reflect crystallization from different REE sources. For example, type-1 florencite may have crystallized largely from REE introduced to the sampled zone, whereas type-2 florencite could have formed early from REE originally present in the granite. This origin is consistent with its chondrite-normalized REE pattern (Figure 10), which resembles that of the unweathered granite. The coexistence of these minerals does not appear to be attributable to an evolutionary sequence, such as described by Altschuler (1973), inasmuch as no overall trend in relative REE abundances has been noted with increasing weathering (Figure 12).

Cerium fractionation

The behavior of Ce differed significantly from that of the other REE, as reflected in the notably low Ce content of three of the four alteration products of apatite analyzed. Type-2 florencite was the only identified apatite alteration product that contained appreciable Ce. Calculations based on the analysis of weathered biotite presented in Table 4 show that in granite containing 10% vermiculitized biotite, inclusions in this mineral can account for only 8% of the Ce in the rock, suggesting that type-2 florencite is scarce. On the basis of the Ce contents of fresh and weathered biotites (see Table 4), very little Ce was apparently introduced into the biotite during weathering, indicating that the Ce content of type-2 florencite was derived from sources within the biotite, probably apatite.

Ce is strongly concentrated in clay-size (<2 μm) materials (Table 2 column 5; Figure 13). Most of the REE

https://doi.org/10.1346/CCMN.1989.0370202 Published online by Cambridge University Press

Table 4. Neutron activation analyses of fresh and weathered granites, clay fractions, and biotites.

	Island Bend			Bemboka profile: whole rock						Bemboka clay fraction			Bemboka biotite	
	IB 1	IB 6	IB 6	BEM 1	BEM 2	BEM 3	BEM 4	BEM 5	BEM 6					
Element	Fresh	Weathered	Clay	Fresh		Slightly weathered		Most weathered		BEM 4	BEM 5	BEM 6	BEM 1	BEM 4
wt. %														
Na_2O	2.94	0.55	0.89	2.89	2.34	1.10	0.94	0.52	0.33	1.89	1.04	1.20	0.27	2.24
FeO	2.75	3.10	2.26	2.90	2.73	2.98	2.98	3.00	3.53	4.81	5.24	7.97	24.59	20.00
ppm														
Sc	9.71	11.81	12.30	11.02	10.73	12.34	12.01	11.74	11.60	21.67	21.97	27.11	69.43	64.65
Cr	5.86	5.87	4.40	8.82	4.90	3.18	4.51	5.24	2.40	7.85	5.72	6.08	43.91	41.87
Rb	104.21	133.96	81.55	161.55	151.81	173.65	178.63	171.92	176.26	136.21	98.44	106.48	456.10	445.01
Sb	0.01	0.06	0.53	0.14	0.15	0.19	0.05	0.08	0.23	0.10	0.35	0.80	0.03	0.52
Cs	4.70	5.05	4.80	5.89	5.39	5.71	7.02	6.90	6.51	12.37	10.57	9.79	29.33	29.75
Ba	791.95	1009.57	713.89	699.87	675.97	935.80	837.00	812.50	808.10	1277.27	1082.33	1169.77	3393.40	2833.64
La	24.54	42.86	39.75	41.28	336.20	573.90	341.00	376.80	411.60	615.60	620.60	634.20	18.20	1768.70
Ce	45.51	57.54	87.02	86.52	86.61	77.97	76.61	128.89	124.05	509.39	518.96	487.06	46.26	64.78
Nd	17.52	38.47	30.23	37.04	276.42	496.32	279.13	308.53	345.61	441.94	403.45	430.42	28.76	1554.98
Sm	3.20	7.79	6.78	7.20	60.95	100.50	56.90	61.80	68.00	88.01	81.67	86.28	9.00	323.72
Eu	0.79	2.10	1.98	1.16	10.15	16.34	9.28	10.11	10.96	14.48	13.62	14.09	0.34	48.90
Gd	2.97	7.22	6.91	6.73	63.69	99.36	58.54	63.97	68.42	91.64	85.19	85.65	9.71	283.41
Tb	0.46	1.12	1.18	1.04	8.56	11.57	7.09	8.03	8.79	13.81	12.51	12.85	1.48	29.83
Ho	0.64	1.62	2.03	1.21	11.01	13.33	8.73	10.14	11.35	18.52	17.23	17.89	2.76	36.37
Yb	2.02	5.12	5.75	3.82	22.56	28.55	20.64	23.44	25.36	43.28	38.16	39.33	7.43	79.24
Lu	0.32	0.82	0.88	0.56	3.36	4.18	3.12	3.55	3.85	6.40	5.63	5.82	1.15	11.70
Hf	2.07	2.29	2.15	5.47	5.10	5.61	5.61	6.00	6.95	2.82	2.16	2.98	10.69	17.63
Ta	1.55	0.86	0.69	1.57	1.02	0.71	0.41	0.53	0.75	1.02	0.90	1.14	3.89	1.68
Th	9.29	10.67	12.07	22.61	18.91	19.69	20.82	21.08	25.59	86.32	67.35	76.30	9.91	28.84
U	2.66	3.05	6.49	4.47	3.84	4.28	2.96	2.84	3.67	9.01	7.03	7.53	6.37	7.79

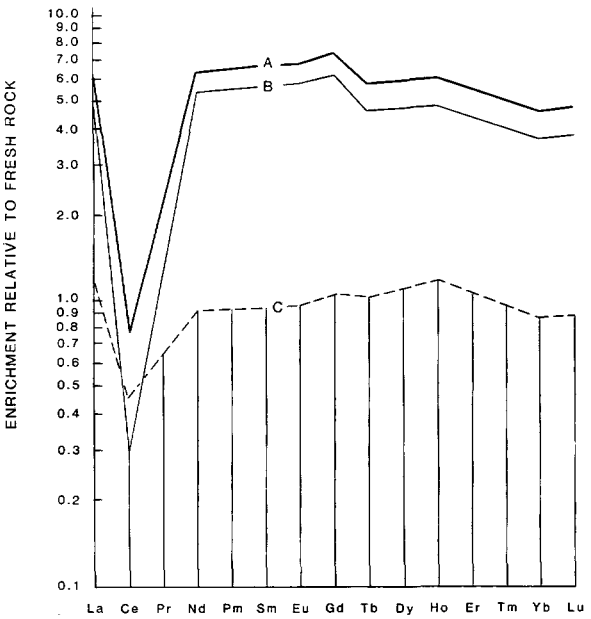

Figure 13. Distribution of rare earth elements between the clay and non-clay fractions of Bemboka 4. A = total enrichment in the sample; B = enrichment in the non-clay fraction; C = enrichment in the clay-size fraction.

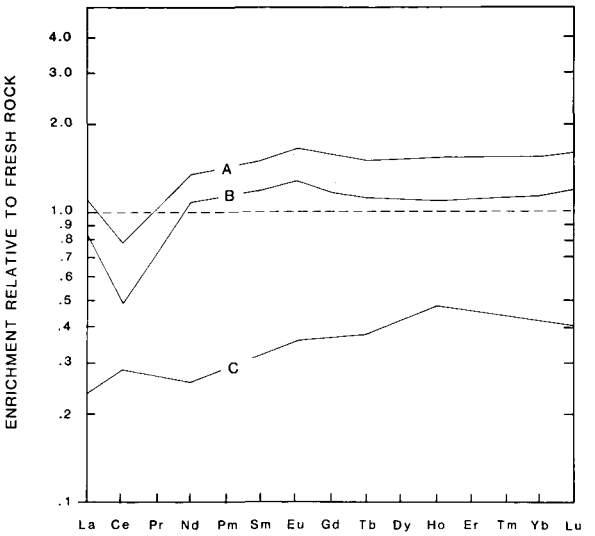

Figure 14. Enrichment of rare earth elements in strongly weathered Island Bend (IB 6) granite (A); non-clay fraction of IB 6 (B); and clay fraction of IB 6 (C). Dashed line represents result if abundance (ppm/cm³) of each rare earth element in IB 6 is equal to that in fresh granite.

(particularly LREE) in the fresh granite are hosted by allanite. Optical examination of this mineral indicated that it weathered to red-brown material, the electron diffraction patterns from which contained a few broad, diffuse rings. Thus this Ce-rich, finely crystalline material probably was concentrated in the clay-size fraction.

The fractionation of Ce from trivalent REE in sea water by oxidation and precipitation as CeO_2 was originally suggested by Goldberg (1961). This concept, supported by Ludden and Thompson (1979) and Elderfield *et al.* (1981), suggests that Ce has a relatively low solubility in meteoric water. Under the oxidizing conditions that prevail during weathering of the Bemboka granodiorite, the formation of a quadrivalent species drastically reduced the mobility of Ce, explaining the strong fractionation of this element from the other REE observed in this study.

Table 5. Distribution of rare earth elements (% of total) in secondary phosphate minerals after apatite.

	Residual in biotite	In clay fraction	Not accounted for
La	52	16	32
Ce	8	62	30
Nd	56	14	30
Sm	57	14	29
Eu	53	14	33
Gd	48	14	38
Tb	42	18	40
Ho	42	19	39
Yb	38	19	43
Lu	38	18	44

REE enrichment of the weathering profile

The whole rock analyses in Table 4 indicate that the profile was substantially enriched in REE during weathering. As illustrated in Figure 11, the REE contents of weathered granite samples are significantly greater than those of fresh rock, confirming that the replacement of apatite described here was the result of weathering, not of hydrothermal alteration. Figure 12 reveals that the net result of apatite replacement by REE-bearing phases was to enrich most REE to a similar extent, without strong fractionation. Thus, the assemblage added to the profile probably had a REE signature very similar to that of the unweathered rock. REE were probably derived from elsewhere in the weathering granite. Abundances of all REE except Ce appear to peak, and then remain constant through to the final stages studied, reflecting fixation of the REE in minerals that were resistant to further alteration under the conditions encountered in this region. Intervention of erosion at this stage would have produced sediments containing rather insoluble REE-phosphate minerals (log $K_{sp}°$ rhabdophane at 25°C is about −24; Jonasson *et al.*, 1985).

Strong enrichment of the Bemboka profile in all REE except Ce implies that under different conditions, such as encountered higher in the profile where organic matter may participate strongly in weathering reactions, secondary REE-bearing minerals must break down. A

https://doi.org/10.1346/CCMN.1989.0370202 Published online by Cambridge University Press

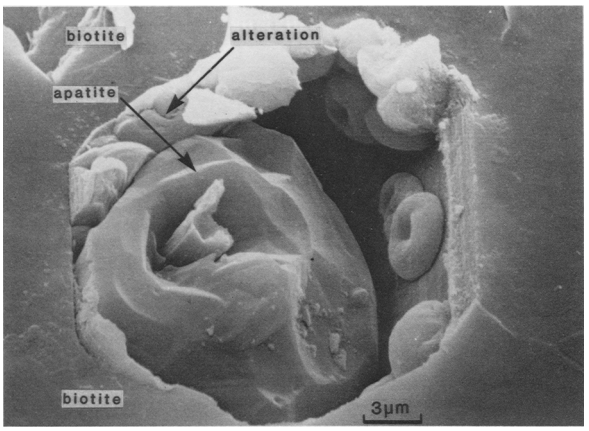

Figure 15. Scanning electron micrograph of partly weathered apatite crystal enclosed in biotite. Apatite has been replaced by material that locally displays half-donut shapes.

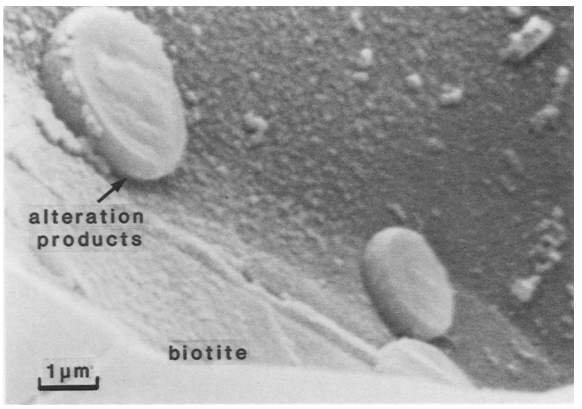

Figure 16. Disk-shaped rare earth phosphate minerals in a hexagonal pit in biotite from Island Bend granite.

similar process was described by Altschuler *et al.* (1958) and Altschuler (1973), who reported secondary enrichment of U in crandallite and apatite, apparently as the result of expulsion of U from crandallite as it was converted to wavellite in an upper zone.

The similarity between the shapes of the enrichment plots of the biotite and whole rock in Figure 12 supports the conclusion that apatite replacement within biotite crystals controlled the distribution of REE in the weathered rock; however, the biotite plot is more enriched in LREE than that of the weathered granite. Similarly, column 3 of Table 5 indicates that a higher proportion of the HREE (than MREE and LREE) can not be accounted for by apatite replacement in biotite or the clay fraction. Together, these observations suggest crystallization of a more HREE-enriched weathering product not enclosed within biotite.

Behavior of P, Ba, Th, Hf, U, and Sb

The P_2O_5 contents of samples from the Bemboka weathering profile range from 0.05% in fresh granite to 0.01–0.02% in strongly weathered samples (Banfield, 1985), indicating that about 85% of the P originally present was removed from the profile in solution during weathering. This loss is reflected by the small volume of alteration products relative to parent apatite and the presence of obvious solution pits in apatite in moderately weathered granite.

None of the other trace elements analyzed were strongly enriched in the weathering profile. Although Ba was concentrated in the apatite replacement phases, it was apparently derived from the surrounding biotite. This enrichment is most clearly demonstrated by the data in Table 4, which indicate that the Ba content of the weathered biotite is actually lower than that of the fresh biotite. Th, and to a lesser extent Hf, U, and possibly Sb, were concentrated in the weathered biotite (presumably in apatite replacement phases), although these elements were lost overall during weathering.

Role of organisms

Organisms such as bacteria were possibly involved in the formation of donut-shape apatite replacement products. Lucas and Prévôt (1985) and Prévôt and Lucas (1986) synthesized apatite using microorganisms. Lucas and Prévôt (1985) reported the formation of microspheres having a size range similar to that of the donut-shape particles and that occurred as chains and aggregates having a radial structure. They suggested that the microspheres may have been mineralized organisms either directly conserved or serving as seeds for further crystallization. We have no evidence to indicate that microorganisms were responsible for the donut shape of aggregates, other than their strong morphological resemblance to those reported by Lucas and Prévôt (1985). The formation of replacement rims containing half-donut shapes and tiny aggregates nucleated on apatite surfaces, such as illustrated in Figure 15, the range of euhedral crystals of replacement minerals (Figures 3e, 3f, 7, and 9), and the high REE content suggest crystallization by an inorganic process. If organisms were involved in the formation of the donut-shape aggregates, they have been replaced in every sample examined.

Apatite weathering in the Island Bend profile

In the Island Bend profile apatite weathering was characterized by the development of crystallographically controlled etch pits and the formation of small quantities of a secondary mineral (Figure 16). Qualitative EDX analyses of this material indicated that it was composed chiefly of LREE and P. Although insufficient material was available for further identification of the alteration products, these observations complement those on samples from the Bemboka profile.

https://doi.org/10.1346/CCMN.1989.0370202 Published online by Cambridge University Press

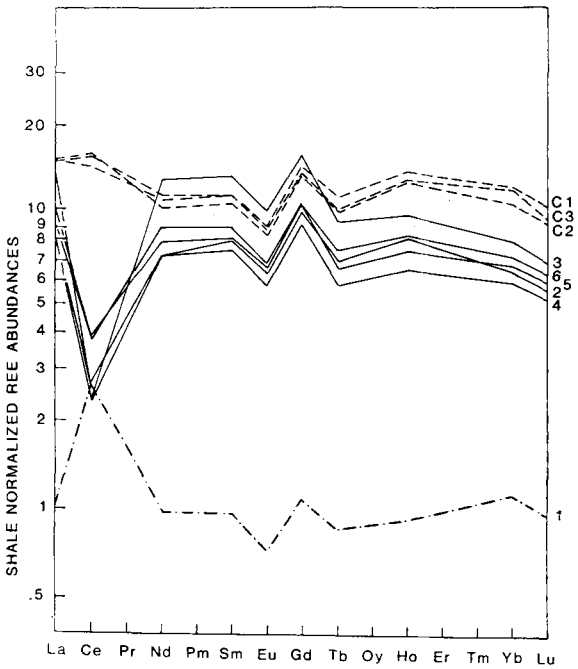

Figure 17. Shale-normalized rare earth abundances in (1) fresh, (2) slightly weathered, (3, 4) moderately weathered, and (5, 6) strongly weathered Bemboka granite and in clay fractions from (4), (5), and (6). Shale rare earth contents from Haskin and Haskin (1966).

APPLICATIONS

Studies of the REE contents of sediments have been used to examine aspects of their origin (e.g., Piper, 1974) and to contribute to an understanding of crustal evolution (e.g., Wildeman and Haskin, 1973; Nance and Taylor, 1976). The form and distribution of REE in these sediments must be controlled in part by reactions which occur at the weathering front.

Shale-normalized REE patterns for fine-grained sediments are characterized by a positive Ce anomaly, whereas coarser grained sediments are associated with a negative Ce anomaly (Tlig, 1982). In Figure 17, clay and whole rock abundances for the Bemboka granite have been normalized to shale using data from Haskin and Haskin (1966). Although the positive Ce anomaly in the clay fraction in Figure 17 appears to be small, it should be noted that the REE pattern for this fraction is partly controlled by apatite alteration products which superimpose a strong negative Ce anomaly. The clear association of Ce with the clay fraction suggests that the distribution of Ce between fine and coarser fractions is a characteristic which developed during weathering.

On the basis of experimental data using concentrated solutions, Jonasson *et al.* (1985) showed that LREE react with fluorapatite surfaces. They proposed that rhabdophane and hydrous xenotime are important phases in controlling REE concentrations in the oceans. Their model involved reprecipitation of metastable surface-adsorbed REE as insoluble REE-phosphates. Our study suggests that under certain conditions, REE abundances in sediments will be controlled directly by phosphate minerals formed at the weathering front.

The formation of REE-phosphate minerals after apatite and the inclusion of these phases into sediments provides a mechanism to explain the presence of monazite in the source regions of S-type (Chappell and White, 1974) granitic rocks (Sawka *et al.,* 1986). Refractory monazite may represent an important source of deep-crustal radioactive-heat (Sawka and Chappell, 1986) and a means of controlling the distribution of Th, Nd, decay products, and other REE in rocks which have undergone chemical weathering (Sawka *et al.,* 1986).

The phosphorus content is critical in determining soil fertility. Because of low atmospheric returns, this element must be supplied almost entirely by the parent material. Plumbogummite minerals [$XAl_3(PO_4)_2(OH)_5H_2O$; X = (Pb, Ca, Sr, Ba, Ce, REE)] have been identified in soils by several workers (e.g., Norrish, 1968; Adams *et al.,* 1973; Bottinnelly, 1976). These relatively insoluble minerals have almost certainly formed by a process of apatite replacement, similar to that described above.

The considerable mobility of REE during the early stages of weathering is of significance to studies of changes in profile and soil geochemistry. Conclusions should not be based on calculations which assume that components such as the REE or Y (which in the profiles studied follows the trivalent REE) are immobile during alteration. Of the REE, only Ce does not appear to be strongly redistributed during weathering in these profiles. The weathering process also appears to be capable of fractionating Nd from Sm (Figure 10). The observation that this fractionation occurs relatively early in weathering may be of significance, for example, to Nd/Sm studies of partly altered rocks and sedimentary material.

ACKNOWLEDGMENTS

We thank B. Hyde of the Research School of Chemistry for access to the transmission electron microscope and D. Goodchild for access to the scanning transmission electron microscope, P. Barlow and J. Preston for technical assistance, L. Widmeier for drafting, B. Chappell of the Geology Department for neutron activation analyses, and N. Ware of the Research School of Earth Sciences for assistance with CAMECA microprobe determinations. D. R. Veblen, K. J. T. Livi, D. A. Sverjensky, Z. Altschuler, and P. Moore are thanked for their critical reviews of the manuscript.

REFERENCES

Adams, J. A., Howarth, D. T., and Campbell, A. S. (1973) Plumbogummite minerals in a strongly weathered New Zealand soil: *J. Soil Sci.* **24,** 225–231.

Altschuler, Z. S. (1973) The weathering of phosphate deposits—Geochemical and environmental aspects: in *Environmental Phosphorus Handbook,* J. Griffith, ed., Wiley-Interscience, New York, 718 pp.

Altschuler, Z. S., Clarke, R. S., and Young, E. J. (1958) Geochemistry of uranium in apatite and phosphorite: *U.S. Geol. Surv. Prof. Pap.* **314-D,** 45–90.

Banfield, J. F. (1985) The mineralogy and chemistry of granite weathering: M.Sc. thesis, Australian National University, Canberra, Australia, 229 pp.

Bottinelly, T. (1976) A review of the minerals of the alunite-jarosite, beudantite, and plumbogummite groups: *J. Res. U.S. Geol. Surv.* **4,** 213–216.

Bowles, J. F. W. and Morgan, D. J. (1984) The composition of rhabdophane: *Mineral. Mag.* **48,** 146–148.

Burkov, V. V. and Podporina, E. K. (1967) Rare earths in the weathering crusts of granitoids: *Dokl. Akad. Nauk S.S.S.R.* **177,** 691–694.

Chappell, B. W. and White, A. J. R. (1974) Two contrasting granite types: *Pacific Geology* **8,** 173–174.

Duddy, I. R. (1980) Redistribution and fractionation of rare earth and other elements in a weathering profile: *Chem. Geol.* **30,** 363–381.

Elderfield, H., Hawkesworth, C. J., and Greaves, M. J. (1981) Rare earth element geochemistry of oceanic ferromanganese nodules and associated sediments: *Geochim. Cosmochim. Acta* **45,** 513–528.

Flicoteaux, R. and Lucas, J. (1984) Weathering of phosphate minerals: in *Phosphate minerals,* J. O. Vriega and D. B. Moore, eds., Springer-Verlag, Berlin, 292–317.

Gardner, L. R., Kheoruenromne, I., and Chen, H. S. (1978) Isovolumetric investigations of a buried granite saprolite near Columbia, South Carolina: *Geochim. Cosmochim. Acta* **42,** 417–424.

Gardner, L. R., Kheoruenromne, I., and Chen, H. S. (1981) Geochemistry and mineralogy of an unusual diabase saprolite near Columbia, South Carolina: *Clays & Clay Minerals* **29,** 184–190.

Goldberg, E. D. (1961) Chemistry in the oceans: in *Oceanography,* M. Sears, ed., Amer. Assoc. Adv. Sci., Washington, D.C., 583–593.

Hanson, G. N. (1980) Rare earth elements in petrogenetic studies of igneous systems: *Ann. Rev. Earth Plan. Sci.* **8,** 371–406.

Harris, C. (1985) Guano-derived rare earth-rich phosphatic amygdales in gabbroic inclusions from Ascension Island: *Earth Planet. Sci. Letters* **72,** 141–148.

Haskin, M. A. and Haskin, L. A. (1966) Rare earths in European shales: A redetermination: *Science,* **154,** 507–509.

Jonasson, R. G., Bancroft, G. M., and Nesbitt, H. W. (1985) Solubilities of some hydrous REE phosphates with implications for diagenesis and sea water concentrations: *Geochim. Cosmochim. Acta* **49,** 2133–2139.

Krasil'nikov, A. V. (1969) Behavior of rare elements in weathering profiles developed on granitic rocks: *Geol. Razedka,* 141–142. (Russian). Examined in *Chem. Abst.* **75,** 90186.

Lucas, J. and Prévôt, L. (1985) The synthesis of apatite by bacterial activity: Mechanism: *Sci. Géol. Mém.* **77,** 83–92.

Ludden, J. N. and Thompson, G. (1979) An evaluation of the behavior of the rare elements during the weathering of sea-floor basalt: *Earth and Planet. Sci. Lett.* **43,** 85–92.

Mooney, R. C. L. (1950) X-ray diffraction study of cerous phosphate and related crystals. 1. Hexagonal modification: *Acta. Crystallogr.* **3,** 337–341.

Nance, W. B. and Taylor, S. R. (1976) Rare earth element patterns and crustal evolution. 1. Australian post-Archean sedimentary rocks: *Geochim. Cosmochim. Acta* **40,** 1539–1551.

Nance, W. B. and Taylor, S. R. (1977) Rare earth element patterns and crustal evolution. 2. Archean sedimentary rocks from Kalgoorlie, Australia: *Geochim. Cosmochim. Acta* **41,** 225–231.

Nesbitt, H. W. (1979) Mobility and fractionation of rare earth elements during weathering of a granodiorite: *Nature* **279,** 206–210.

Norrish, K. (1968) Some phosphate minerals in soils: in *Trans. 9th Conf. Int. Soil Sci. Soc., Adelaide Vol. 2,* J. W. Holmes, ed., Elsevier, New York, 713–723.

Piper, D. Z. (1974) Rare earth elements in the sedimentary cycle: A summary: *Chem. Geol.* **14,** 285–304.

Prévôt, L. and Lucas, J. (1986) Microstructure of apatite replacing carbonate in synthesized and natural samples: *J. Sed. Pet.* **56,** 153–159.

Sawka, W. N., Banfield, J. F., and Chappell, B. W. (1986) A weathering-related origin of widespread monazite in S-type granites: *Geochim. Cosmochim. Acta* **50,** 171–175.

Sawka, W. N. and Chappell, B. W. (1986) The distribution of radioactive heat production in I- and S-type granites and residual source regions: Implications to high heat flow areas in the Lachlan Fold Belt, Australia: *Aust. J. Earth Sci.* **33,** 107–118.

Tlig, S. (1982) Distribution des terres rares dans les factions de sédiments et nodules de Fe et Mn associés en l'océan: *Marine Geology* **50,** 257–274.

Vlasov, K. A., ed. (1966) *Geochemistry and Mineralogy of Rare Elements and Genetic Types of Their Deposits. Vol. III, Mineralogy of the Rare Elements:* Translated by Z. Lerman, Israel Prog. for Sci. Transl., Jerusalem, 945 pp.

Wildeman, T. R. and Haskin, L. A. (1973) Rare earths in Precambrian sediments: *Geochim. Cosmochim. Acta* **37,** 429–438.

(Received 29 October 1985; accepted 8 October 1988; Ms. 1532)